Med-GLIP: Advancing Medical Language-Image Pre-training with Large-scale Grounded Dataset

Zive Deng* Zhejiang University Hangzhou, China

Ruihan He* Zhejiang University Hangzhou, China

Jiaxiang Liu* Zhejiang University Hangzhou, China

Yuan Wang* Zhejiang University Hangzhou, China ziye.21@intl.zju.edu.cn ruihanhe021@gmail.com jiaxiang.21@intl.zju.edu.cn yuanwang23@zju.edu.cn

Zijie Meng Zhejiang University Hangzhou, China

Songtao Jiang Zhejiang University Hangzhou, China zijie.22@intl.zju.edu.cnsongtao.22@intl.zju.edu.cn

Yong Xie Nanjing University of Posts and Telecommunications Nanjing, China yongxie@njupt.edu.cn

Zuozhu Liu Zhejiang University Hangzhou, China zuozhuliu@intl.zju.edu.cn

Abstract-Medical image grounding aims to align natural language phrases with specific regions in medical images, serving as a foundational task for intelligent diagnosis, visual question answering (VQA), and automated report generation(MRG). However, existing research is constrained by limited modality coverage, coarse-grained annotations, and the absence of a unified, generalizable grounding framework. To address these challenges, we construct a large-scale medical grounding dataset Med-GLIP-5M comprising over 5.3 million region-level annotations across seven imaging modalities, covering diverse anatomical structures and pathological findings. The dataset supports both segmentation and grounding tasks with hierarchical region labels, ranging from organ-level boundaries to fine-grained lesions. Based on this foundation, we propose Med-GLIP, a modalityaware grounding framework trained on Med-GLIP-5M. Rather than relying on explicitly designed expert modules, Med-GLIP implicitly acquires hierarchical semantic understanding from diverse training data-enabling it to recognize multi-granularity structures, such as distinguishing lungs from pneumonia lesions. Extensive experiments demonstrate that Med-GLIP consistently outperforms state-of-the-art baselines across multiple grounding benchmarks. Furthermore, integrating its spatial outputs into downstream tasks, including medical VQA and report generation, leads to substantial performance gains. Our dataset will be

Index Terms—Medical Dataset, Medical Image Grounding, **Grounded Language-Image Pre-training**

I. INTRODUCTION

With the rapid progress of medical AI, establishing precise alignment between natural language descriptions and specific regions in medical images has become a foundational step for tasks such as intelligent diagnosis, surgical navigation, and multimodal question answering [1]-[9]. Medical image grounding aims to localize anatomical structures or pathological findings based on language input, enabling spatial-semantic correspondence across modalities. For example, when a radiologist states "a tumor is located in the upper right corner," the model must accurately identify the corresponding image region. This task not only improves model interpretability but also provides critical spatial priors for downstream applications like visual question answering (VQA) and medical report generation (MRG), playing an essential role in clinical decision support [9]–[16]

However, compared to the natural image domain, medical image grounding faces several unique challenges [17], [18]. First, publicly available grounding datasets are extremely scarce, especially those with large-scale, multi-organ, and multi-modality annotations, which significantly limits progress in this field. Second, medical images are highly specialized, and exhibit substantial heterogeneity across modalities such as CT, MRI, and ultrasound—in terms of spatial resolution, anatomical appearance, and contrast-making cross-modal alignment inherently complex [19]–[21]. Moreover, many target regions, such as small lesions or vascular branches, often lack clear boundaries and exhibit high anatomical variability, placing greater demands on the model's precision and generalization capabilities.

To address data scarcity and semantic misalignment in medical image grounding, prior works have explored both dataset construction and cross-modal modeling. On the dataset side, SLAKE [1] offers region-phrase annotations for chest Xrays, marking an early attempt at grounding but with only 6k samples and limited modality coverage. MedTrinity-25M [22] provides large-scale but loosely aligned image-text pairs across tasks, lacking fine-grained region-level supervision. These datasets commonly suffer from: (1) limited modality and organ diversity; (2) absence of dense region-level annotations; and (3) a focus on classification or QA tasks rather than spatialsemantic alignment. On the modeling side, recent approaches adapt natural-image cross-modal models to the medical domain (e.g., LLaVA-Med [23], MedKLIP [24], MedSAM [25]), often with structured medical knowledge. LLaVA-Med [23] introduces multimodal LLMs but relies on image-caption

TABLE I: Unified comparison of medical image grounding datasets. BB = bounding-box, 3D-BB = volumetric BB, EP = extreme-point supervision, ROI = region-of-interest. $\sqrt{\mbox{\sc k}}$: support / not supported.

Dataset	Year	RoI Scale	Annotation Type	Multi-modal	Seg.	Ground	≥100K	Coverage / Highlight
VQA-RAD	2018	N/A	None	Х	X	Х	Х	Common pathologies; QA
SLAKE	2021	642 images	Mask	X	\checkmark	×	X	7 organ categories; QA + segmentation
MS-CXR	2022	1162 images	BB	X	X	\checkmark	X	8 thoracic findings
CT-RAD	2023	10410 studies	3D-BB	X	X	\checkmark	X	Volumetric abnormalities
MedTrinity-25M	2024	_	BB / Mask	\checkmark	\checkmark	✓	×	>15 organs, multimodal reports
Med-GLIP-5M	2025	5.3M pairs	BB / Mask	\checkmark	\checkmark	\checkmark	\checkmark	7 modalities, 30+ anatomical regions

pairs without fine-grained alignment. MedKLIP [24] employs region-phrase contrastive learning but remains X-ray-specific. MedSAM [25] incorporates structure-aware priors for zero-shot organ segmentation based on SAM [26], yet depends on prompts and lacks deep language grounding. OntoRay further integrates radiological ontologies to capture causal relations between terms and regions [27]. Despite these efforts, a unified, modality-adaptive grounding framework capable of multiscale semantic alignment and inter-modality generalization is still missing, and its impact on downstream tasks such as VQA or report generation remains underexplored.

To address these challenges, we first propose Med-GLIP-5M, a large-scale medical grounding dataset comprising over 5.3 million region-level annotations across seven imaging modalities, covering diverse anatomical structures and pathological findings. We first construct a comprehensive dataset containing over 5.3 million region-level annotations across seven imaging modalities and dozens of anatomical and pathological categories (Table I). This dataset is curated from multiple public medical segmentation sources and is characterized by three key properties: segmentability, groundability, and multi-granularity. We have standardized and refined the data processing to ensure it adheres to data usage regulations and ethical considerations. Based on this foundation, we also proposed Med-GLIP, which adopts a hierarchical expert paradigm, where dedicated grounding modules are trained for each imaging modality, enabling accurate localization of fine-grained anatomical structures (Figure 4). Furthermore, we demonstrate that incorporating Med-GLIP's grounding outputs into downstream tasks-such as medical VQA and report generation—leads to significant performance improvements, highlighting the value of explicit spatial grounding for multimodal medical reasoning. In summary, our contributions are as follows:

- To the best of our knowledge, we introduce the largest and most diverse medical grounding dataset to date, Med-GLIP-5M, spanning 7 modalities, 30+ anatomical regions, and over 5.3 million image-text region pairs, addressing the long-standing data scarcity in this field.
- We propose Med-GLIP, a modality-aware hierarchical expert framework that enables high-precision grounding across diverse medical imaging types by modeling finegrained structural differences.
- Through extensive experiments, we validate the effectiveness of spatial grounding in downstream tasks, showing that Med-GLIP enhances both VQA and report generation

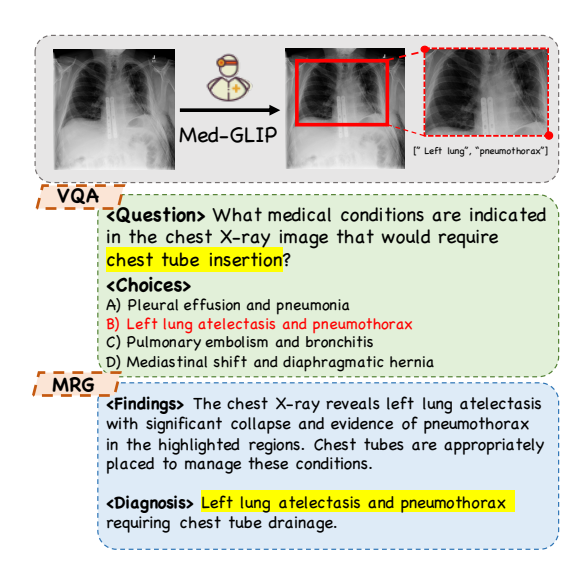


Fig. 1: Enhance VQA and MRG with Med-GLIP.

performance. Our work provides a unified solution across data, modeling, and application perspectives, advancing the development of generalizable medical vision-language models.

II. MED-GLIP-5M CONSTRUCTION

A. Data Source Analysis

In this study, we curated a comprehensive medical image dataset by aggregating resources from multiple platforms, including publicly available repositories such as GitHub, Grand Challenge, OpenNeuro, SYNAPSE, and BraTS, as well as expert annotations provided by collaborating clinicians from affiliated hospitals. The collected datasets span a wide range of imaging modalities, spatial resolutions, and anatomical regions, ensuring diversity across organs and clinical tasks, as shown in Figure 2. A key principle in our data collection strategy was to include images with multiple segmentation masks wherever possible, enabling multi-label learning and enhanced contextual understanding.

Following data acquisition, we conducted a systematic preprocessing workflow. Datasets were first categorized by organ type and sorted in ascending order of data volume. Duplicated samples and low-quality data—such as images with insignificant mask coverage or corrupted annotations—were filtered out. To resolve label inconsistency, semantically similar class names were standardized into a unified naming

scheme. For the remaining clean data, we computed bounding boxes (BBox) from the segmentation masks and enriched each dataset with metadata including label names, modality type, dataset size, and mask-image pairing integrity, as shown in Figure 3 and Figure 4.

Finally, all processed datasets were merged and reformatted into a unified metadata repository conforming to the COCO standard. This consolidated dataset serves as the foundation for training our Med-GLIP model, enabling robust and scalable medical vision-language learning across heterogeneous clinical data sources.

B. Data Collection

We curated a multi-source medical imaging dataset for vision-language grounding. Each image was selected with a preference for multi-instance spatial annotations—either multiple masks or bounding boxes per image—thus ensuring the resulting dataset is well-suited for vision-language grounding tasks. Datasets were extracted from several platforms including but not limited to: GitHub, Grand Challenge, OpenNeuro, BraTS, SYNAPSE, and CodaLab. Selection criteria: (1) DICOM/NIfTI accessibility; (2) spatial annotations (masks/bounding boxes); (3) coverage of multiple anatomical regions. This yielded 2720979 images spanning X-ray, CT, MRI across multiple organs including abdomen(32.8%), bone(23.9%), head(17.3%), chest(7.6%) etc. The final dataset has 4.13 masks/image on average, with various modality including CT(61.84%), MRI(26.71%), Ultrasound(1.44%), X-RAY(0.22%), Dermoscopy(0.21%), Endoscopy(0.09%), Fundus(0.09%).

C. Data Quality Control

A three-tier quality control (QC) pipeline was implemented post-collection. Firstly, all DICOM images underwent dcm2niix (v1.0) with --check-mosaic flag. Nonreadable or broken files were discarded. 3D dataset were sliced into 2D on different axis to improve the available data quantity. We standardized the image format across datasets to PNG, while preserving the original resolution to maintain fidelity with source annotations. Secondly, each image was verified to have a corresponding segmentation mask. We implemented format-specific matching scripts to ensure annotation-visual alignment. Samples lacking a valid associated mask were excluded from further processing. Thirdly, we filtered inconsistent annotations: entries with malformed structure, undefined label semantics, or ambiguous mappings were excluded. Moreover, we removed samples where the annotated mask covered only a negligible portion of the image (empirically set as 1.5% area exclusion according PASCAL VOC min IoU standard), as such cases do not provide meaningful spatial grounding for downstream tasks [28]. This quality assurance workflow ensures that only well-structured, clearly labeled, and spatially meaningful samples are retained for model training and evaluation.

D. Data Preprocessing

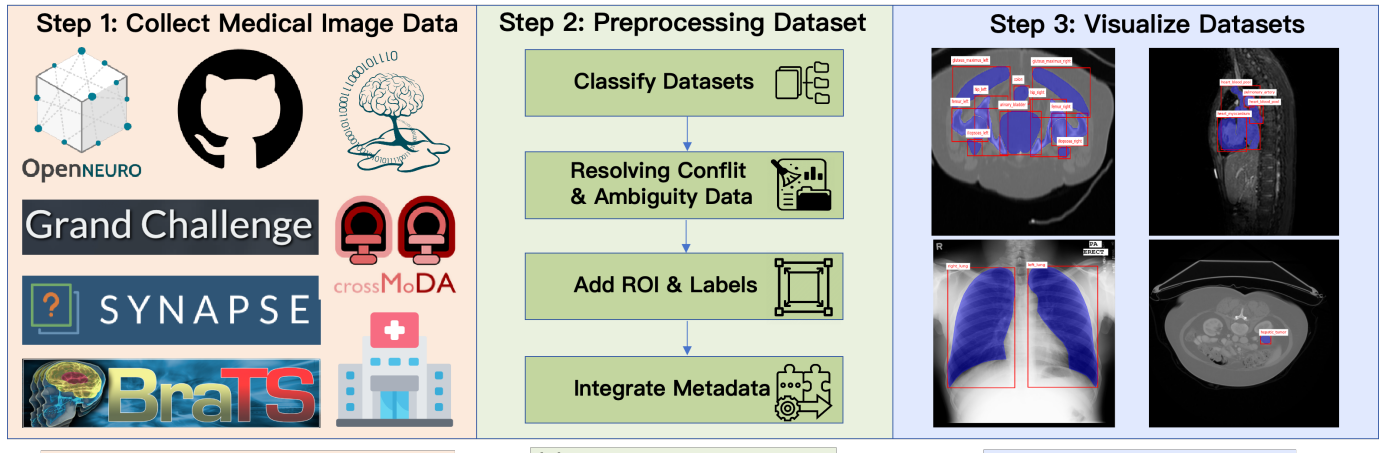
The data preprocessing phase for Med-GLIP-5M was designed to ensure high-quality data while adhering to ethical standards and regulatory requirements. After acquisition, datasets underwent a multi-stage refinement process. Initially, data were categorized by organ type and volume, with duplicates and low-quality samples removed. Semantic label inconsistencies were resolved through standardized naming. Clean data were then augmented with geometric and intensity transformations to enhance diversity without compromising diagnostic integrity. Image formats were standardized to ensure compatibility across machine learning frameworks. A rigorous validation protocol verified the consistency between images and segmentation masks. Additionally, clinical metadata such as patient history and diagnostic outcomes were integrated where available. This structured approach resulted in a dataset that is both large-scale and high-quality, providing a robust foundation for medical AI research.

E. Data Statistics

The dataset used in this study comprises 198 fine-grained annotation labels, which were analyzed via human and reorganized into 38 broader anatomical categories based on label semantics and corresponding dataset documentation by large language models and verified by human. This process, facilitated by large language models and verified by human experts, aimed to enhance anatomical coherence and interpretability for downstream modeling (e.g., mapping specific hip joints to 'pelvis(hip)' and optic components to 'head(eye)'). These 38 hierarchical classes span 6 major body regions, with a cumulative image count exceeding 11 million. Notably, the brain, spine, and abdomen represent the systems with the highest annotation volumes. This hierarchical label structure allows for flexible experimentation across tasks such as organ-level segmentation, multi-organ detection, and facilitates domain adaptation and multi-label learning.

The dataset exhibits substantial heterogeneity with 7 distinct imaging modalities. Computed Tomography (CT) and Magnetic Resonance Imaging (MRI) are predominant, contributing approximately 4.2 million and 1.08 million images, respectively. These two modalities collectively account for over 80% of the total dataset volume. CT scans, reported as constituting 78% among modalities in one analysis, provide extensive coverage across multiple organ systems, including the spine, lung, liver, and kidney. MRI, accounting for 20% among images in a similar context, is particularly enriched in high-resolution brain and neuroimaging data, as well as prostate, cardiac, and vascular regions. The remaining modalities, such as ultrasound, contribute important diversity.

This multimodal composition makes the dataset highly suitable for a broad spectrum of downstream applications, including cross-modal learning, domain adaptation, modality-aware segmentation, and multimodal fusion in disease detection and prognosis. It also enables research into unified frameworks that bridge traditionally distinct clinical domains.



(a)Data Source: 130+ medical datasets

(b)Data Processing Pipeline

(c)Med-GLIP Data Examples

Fig. 2: Overview of the Med-GLIP-5M dataset construction process. (a) Data sources: We collect 129 public medical datasets from diverse platforms including OpenNeuro, Grand Challenge etc. (b) Data preprocessing pipeline: The datasets are categorized, ambiguities resolved, ROIs and textual labels are added, and metadata is integrated into a unified format. (c) Example visualizations of processed data: Our dataset contains fine-grained ROI annotations and corresponding textual descriptions across multiple modalities, supporting region-level grounding and structured understanding.

III. MED-GLIP

In our approach, medical object detection is reconceived as a phrase grounding task, wherein each image region that is identified corresponds to its matching medical phrase. Given a predefined set of medical concepts pertinent to a particular imaging modality, for instance, {"pneumonia", "nodule", "fracture"} for X-ray images, a textual prompt is constructed, such as:

Prompt = "Detect: pneumonia, nodule, fracture".

Following methodologies similar to GLIP [29], we can employ pre-trained language models, e.g., BERT [30], to encode more semantically rich prompts (e.g., "pneumonia. nodule. fracture."), which has demonstrated empirical advantages. Within our modality-specific grounding framework, alignment scores S_{ground} are computed between medical image region features \mathbf{F} and the encoded word or token features \mathbf{T} from the prompt. This is formally expressed as:

$$\mathbf{F} = \operatorname{Enc}_{I}(\operatorname{Img}), \mathbf{T} = \operatorname{Enc}_{L}(\operatorname{Prompt}), S_{\operatorname{ground}} = \sigma(\mathbf{F}\mathbf{T}^{\top})$$
 (1)

where $\mathbf{F} \in \mathbb{R}^{N \times d}$ represents the region features extracted by an image encoder Enc_I , and $\mathbf{T} \in \mathbb{R}^{M \times d}$ denotes the contextual word/token features from a language encoder Enc_L . $\sigma(\cdot)$ represents the sigmoid function for normalization. Each imaging modality (e.g., X-ray, CT, MRI) utilizes a dedicated image encoder $\mathrm{Enc}_{I,\mathrm{modality}}$, while a common language encoder Enc_L is shared across modalities. The grounding model for each modality is trained end-to-end by minimizing the loss function defined in Equation (2), adapted such that the classification logits S_{cls} from Equation (3) are substituted with the computed alignment scores S_{ground} .

$$L_{cal} = L_{cal}^{\text{cls}} + L_{cal}^{\text{loc}}.$$
 (2)

$$\mathbf{F} = \operatorname{Enc}_{I}(\operatorname{Img}), S_{\operatorname{cls}} = \mathbf{F}W^{T}, L_{cal}^{\operatorname{cls}} = loss(S_{\operatorname{cls}}; T),$$
 (3)

Equation (2) and (3) outline the loss computation for a baseline detection model. The model extracts features \mathbf{F} via the image encoder Enc_I and computes classification logits S_{cls} using a classifier weight matrix \mathbf{W} . The total training objective, L_{cal} , is a composite loss comprising two components: (i) a classification loss, L_{cal}^{cls} , calculated from the logits S_{cls} and ground-truth targets \mathbf{T} , and (ii) a localization loss, L_{cal}^{loc} , used for bounding box regression.

To address the potential mismatch between the number of tokens (M) in the encoded prompt and the number of target medical concepts (c), we adopt an expansion strategy analogous to that in GLIP. For a binary sigmoid loss, the ground truth target matrix $\mathbf{T} \in \{0,1\}^{N \times c}$ is expanded into $\mathbf{T}' \in \{0,1\}^{N \times M}$. This expansion involves aligning all sub-word tokens constituting a positive medical phrase to be positive matches (i.e., target value of 1), while any additionally introduced tokens (e.g., punctuation, padding) are designated as negative matches (i.e., target value of 0). During the inference phase, the probability for each medical phrase is derived by aggregating the probabilities of its constituent tokens, typically by averaging. This allows for a flexible and robust mapping from textual prompts to visual detections.

A. Modality-Specific Equivalence.

Within each medical imaging modality, our reformulation establishes a theoretical equivalence between object detection and phrase grounding. By training a grounding model on modality-specific data and prompts, we can directly apply it to detection tasks within that modality in a zero-shot manner, leveraging the rich semantic information encoded in the language prompt.

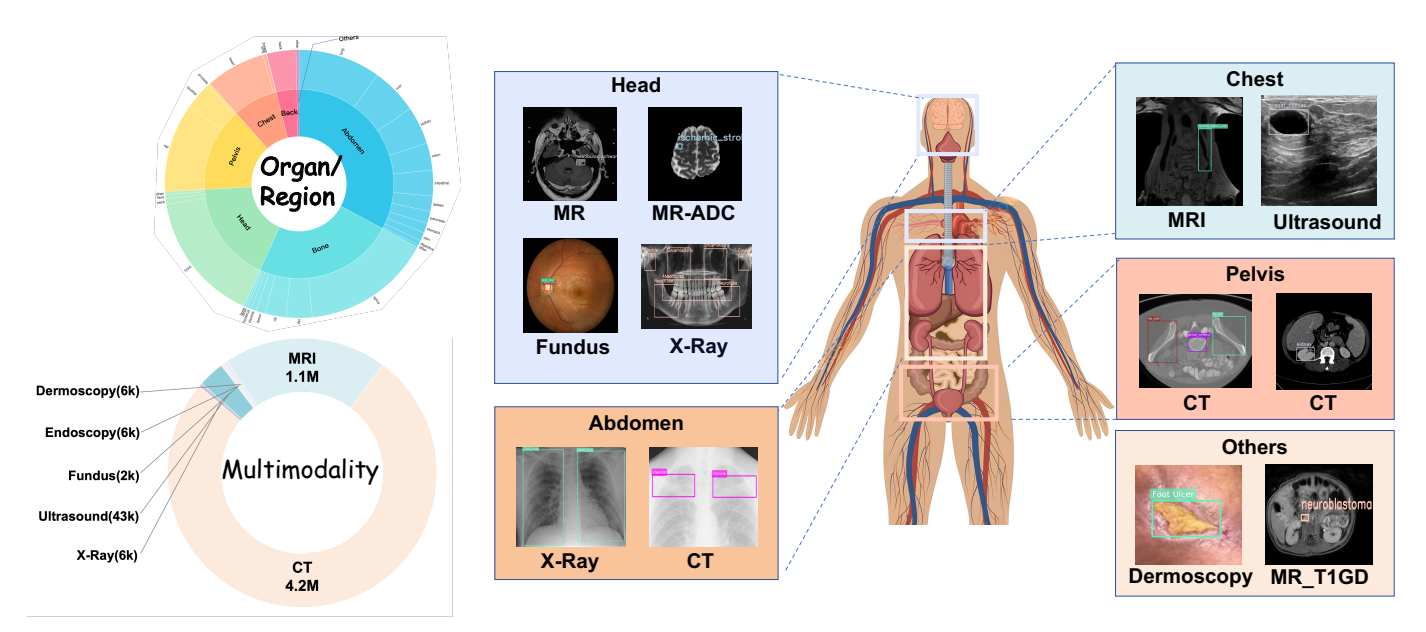


Fig. 3: Med-GLIP-5M has 7 modality categories in total, with multiple organs containing suborgans in the dataset.

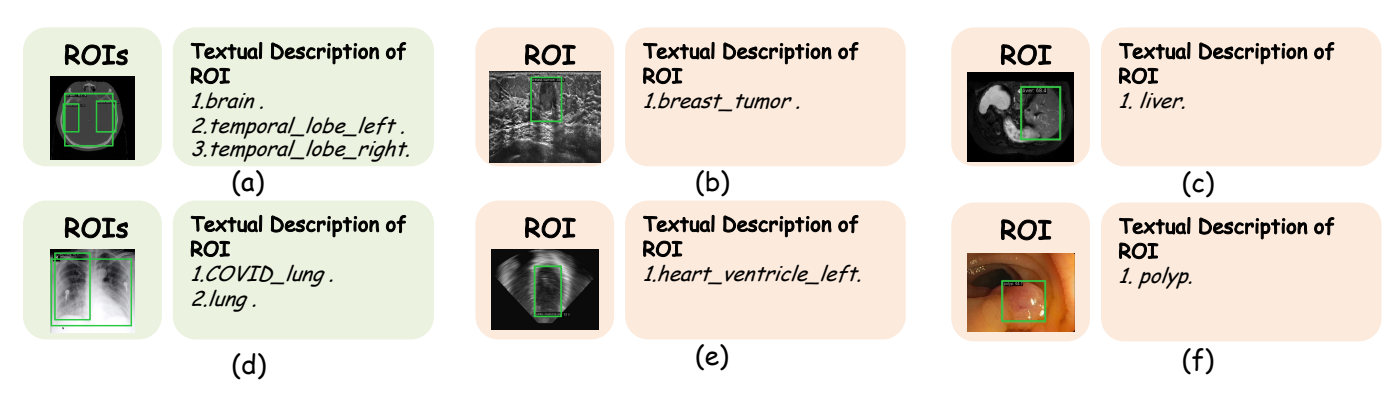


Fig. 4: Illustration of hierarchical region-level annotations across modalities. Each subfigure (a–f) shows green bounding boxes and textual descriptions over CT, X-ray, ultrasound, endoscopy, and MRI images. Multi-level boxes reflect hierarchical semantics, providing fine-grained region-text supervision for structured medical grounding.

IV. EXPERIMENTS

A. Experiment Setup

Datasets for Region-Level Grounding. To evaluate the grounding performance of our GLIP-experts, we selected six datasets spanning five imaging modalities: SegRap2023_ct (CT), AMOS2022_MR (MRI), sz_cxr (X-ray), CETUS2014 (Ultrasound), and CVC-ClinicDB (Endoscopy). All datasets except CVC-ClinicDB are sourced from the IMed-361M benchmark [31], which provides standardized train-test splits (90%/10%). For evaluation, we use only the held-out test sets. CVC-ClinicDB lacks predefined splits and is used in its entirety. These datasets collectively cover 5,551 images with rich structural annotations across modalities.

Datasets for MRG. We adopt two widely-used benchmarks: MIMIC-CXR [32] and IU-Xray [33]. MIMIC-CXR includes 377,110 chest X-ray images and corresponding freetext radiology reports from 227,835 studies. It is evaluated

using the MLRG framework to compute both natural language generation (NLG) metrics and concept grounding scores (e.g., CE). IU-Xray, with 7,470 image-report pairs, offers a smaller and more structured alternative, and is evaluated using the R2Gen model on standard NLG metrics. Datasets for We evaluate model generalization to visionlanguage reasoning via three medical VQA datasets: VQA-RAD [34], SLAKE [1], and PathVQA [35]. These datasets span radiological and pathological domains, include both English and Chinese annotations, and provide over 50,000 QA pairs. During evaluation, GLIP-experts support both: (1) Closed-ended multiple-choice reasoning by verifying spatial alignment between phrases and detected regions; and (2) Open-ended answer generation through grounded semantic reasoning. All evaluations follow official train-test splits for reproducibility and fair comparison.

Baselines and Models. To evaluate the effectiveness of

TABLE II: Performance of different models on grounding tasks across multiple medical imaging modalities. Metrics are Average Precision (AP) and AP@50. "Zero" indicates zero-shot inference; Med-GLIP models are evaluated at 10% and 100% training scale.

Modality	CT		MRI		X-ray		Ultrasound		Endoscopy		Dermoscopy		Fundus Photography	
Representative Dataset	SegRap		AMOS2022		Sz_cxr		CETUS2014		Clinic-DB		Rimonedl		isic2017	
Metric	AP	AP50	AP	AP50	AP	AP50	AP	AP50	AP	AP50	AP	AP50	AP	AP50
GLIP-zero	0.0	0.0	0.0	0.0	0.0	0.0	0.0	0.0	0.0	0.0	0.0	0.0	0.0	0.0
CO_DERT-zero	0.0	0.0	0.0	0.0	0.0	0.0	0.0	0.0	0.0	0.0	0.0	0.0	0.0	0.0
CO_DERT_100%	31.8	38.9	7.6	11.3	69.8	84.2	1.0	7.0	60.4	79.7	43.0	79.5	71.0	87.3
Med-GLIP_10%	41.2	80.7	16.0	43.9	4.9	38.4	9.5	23.5	10.3	33.4	36.0	75.9	14.7	71.3
Med-GLIP_100%	82.7	99.0	28.0	59.2	86.9	100.0	59.2	91.9	33.4	62.5	61.7	90.1	<u>58.8</u>	<u>78.3</u>

our medical bounding box dataset for downstream radiology report generation tasks, we conducted experiments using two representative models: R2Gen and MLRG. R2Gen [36] is a Transformer-based model for medical report generation that uses relational memory and conditional layer normalization. It is a strong and widely used baseline for natural language generation tasks. MLRG [37] is a recent state-of-the-art model that leverages multi-view longitudinal data and contrastive learning. It focuses on clinical accuracy by incorporating patient-specific prior knowledge and advanced multi-modal information.

For Med-VQA tasks, we employed LLaVA-Med [38], a leading large language and vision assistant designed specifically for biomedical applications. This model excels at closedend & open-ended medical visual question answering by effectively integrating visual information from medical images with clinical knowledge.

For the grounding tasks, we compared 5 different models: (1) the original GLIP model without fine-tuning, (2) GLIP experts fine-tuned on modality-specific subsets, (3) GLIP experts fine-tuned on 10% modality-specific subsets, (4) the original CO_DETR model without fine-tuning, and (5) CO_DETR model fine-tuned on modality-specific subsets. GLIP [29] is a vision-language model that unifies object detection and grounding by pre-training on large-scale image-text pairs, enabling open-vocabulary detection and flexible region-text alignment. Co-DETR [39] builds on the DETR architecture and incorporates language queries to perform referring expression grounding using transformers to directly link free-form text with specific image regions.

Implementation Details. All experiments were conducted on an Ubuntu server equipped with 8 NVIDIA RTX 3090 GPUs (24 GB each). For grounding tasks, GLIP and CoDETR were fine-tuned on the Med-GLIP dataset for 30 epochs using the Adam optimizer with a learning rate of 2×10^{-4} and a batch size of 5. For medical report generation, R2Gen was trained for 100 epochs using StepLR scheduling, with a learning rate of 5×10^{-5} for the vision encoder and 1×10^{-4} for other parameters (batch size = 32). MLRG was trained for 50 epochs using AdamW and ReduceLROnPlateau, with a learning rate of 5×10^{-5} , and a batch size of 6.

Evaluation Metric. To evaluate the precision of the grounding model GLIP, we adopted a metric called Average

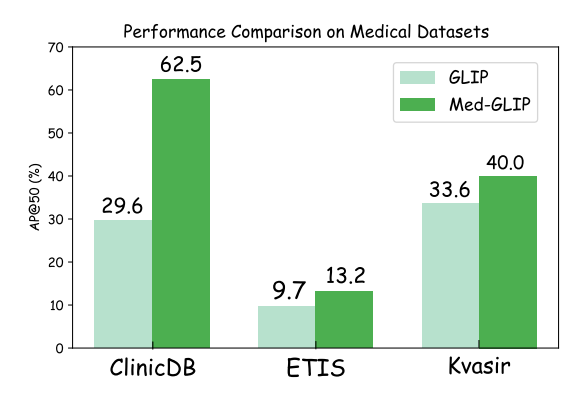


Fig. 5: Performance comparison between GLIP and Med-GLIP on three medical image datasets (ClinicDB, ETIS, and Kvasir) in terms of AP@50. Med-GLIP significantly outperforms the original GLIP model across all datasets, demonstrating the effectiveness of domain adaptation for medical visual grounding tasks.

Precision (AP). AP is a widely used evaluation metric in object detection and grounding tasks. It measures the area under the precision-recall curve, summarizing the trade-off between precision and recall at different confidence thresholds. A higher AP indicates better overall detection or localization performance.

We adopted 2 metrics to evaluate the quality of MRG results: the natural language generation (NLG) metric and the clinical efficacy (CE) metric. The NLG metric quantifies how closely a generated report matches the reference text in terms of linguistic similarity. It includes BLEU-n, METEOR, and ROUGE-L. The CE metric evaluates whether the generated report correctly captures clinically relevant findings and their relationships. It focuses on medical accuracy rather than linguistic overlap. It includes F1 score, Precision (P), and Recall (R). Due to the MLRG model's built-in evaluation module, this project also adopted RadGraph F1 and CheXpert F1. RadGraph F1 measures how accurately a report reproduces clinical entities and their relationships. CheXpert F1 is calculated by labeling the generated medical reports for the presence or absence of fourteen thoracic diseases and then comparing these predictions to the reference labels. For Med-VQA tasks, We employ the accuracy for closed-set questions and recall

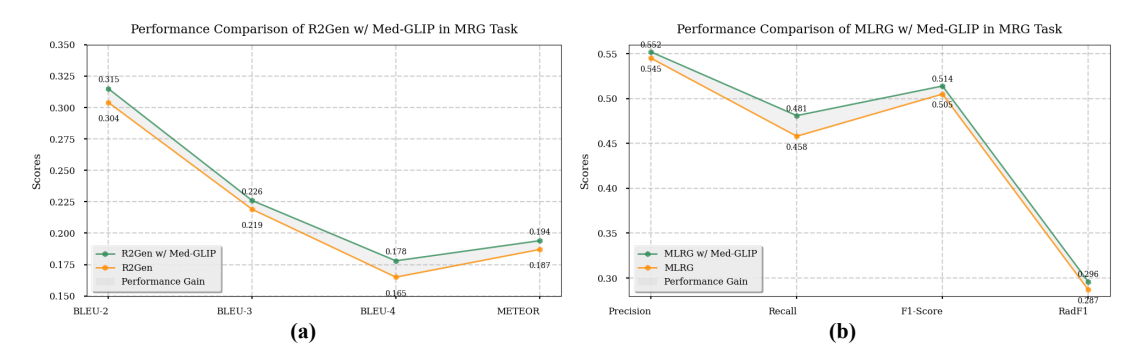


Fig. 6: Performance comparison between w/ and w/o Med-GLIP in MRG Task on the baseline R2Gen and MLRG.

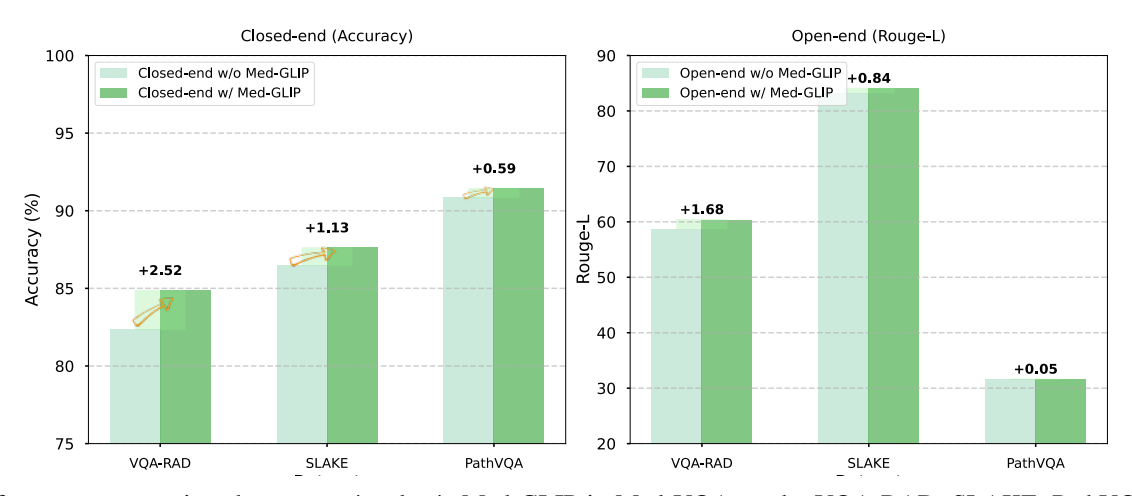


Fig. 7: Performance comparison between w/ and w/o Med-GLIP in Med-VQA on the VQA-RAD, SLAKE, PathVQA Dataset.

for open-set questions, being consistent with existing work like LLaVA-Med [38] for a fair comparison.

B. Results & Analysis

Grounding Performance across Models. As shown in Table II, we first compare the zero-shot grounding performance of GLIP and CO-DETR across all modalities and datasets. Both models achieve near-zero accuracy in this setting, indicating that neither is able to effectively localize medical entities without domain-specific fine-tuning. This demonstrates the substantial domain gap and highlights the necessity of fine-tuning for grounding tasks in medical imaging.

When we finetune Med-GLIP with 10% and 100% of the training data, we observe a clear and consistent improvement in both AP and AP50 metrics across all modalities. For instance, on the CT (SegRap) dataset, AP increases from 0.0 (zero-shot) to 41.2 at 10% scale, and further to 82.7 at 100% scale. Similar trends are observed in X-ray (Sz_cxr), Ultrasound (CETUS2014), endoscopy (Clinic-DB), and other modalities, confirming the effectiveness of our dataset and training strategy in progressively enhancing model performance as more annotated data becomes available.

After full finetuning, Med-GLIP outperforms CO-DETR in five out of seven modalities, including CT, MRI, X-ray, ultrasound, and dermoscopy. For instance, Med-GLIP achieves

substantially higher AP scores on CT (82.7 vs. 31.8), MRI (28.0 vs. 7.6), X-ray (86.9 vs. 69.8), ultrasound (59.2 vs. 1.0), and dermoscopy (61.7 vs. 43.0). Although CO-DETR attains slightly better performance in endoscopy and fundus photography, Med-GLIP demonstrates robust and stable performance across a wider range of modalities, highlighting its strong generalizability and effectiveness as a unified framework for medical grounding tasks. Overall, these results demonstrate that our dataset and adaptation strategy benefit a variety of grounding models, while Med-GLIP in particular achieves the best performance (Figure 5).

Performance of downstream MRG tasks As shown in Figure 6, the enhanced R2Gen model achieved higher BLEU and METEOR scores than its baseline variant, particularly in BLEU4 and METEOR, confirming its ability to generate more semantically aligned reports. However, CE metrics such as Precision, Recall, F1, and RadF1 were not applicable for R2Gen in this setting, as the MIMIC-CXR dataset we used lacks integration with structured clinical annotations.

MLRG demonstrated marked improvements in CE metrics when enhanced with Med-GLIP. These results are attributable to MLRG's capability to utilize bounding box-derived visual features as part of its multi-view contrastive learning and alignment mechanisms. The model's ability to encode clin-

ical dependencies and disease progression pathways further enhanced its factual consistency, as reflected in the CE metrics.

Performance of downstream Med-VQA tasks. As shown in Figure 7, Med-GLIP can enhance the performance of downstream Med-VQA tasks. In closed-end tasks, measured by accuracy, Med-GLIP brings gains across all datasets, with the highest improvement of 2.52% on VQA-RAD. For openend tasks, evaluated by Rouge-L, it also provides consistent boosts, achieving a maximum uplift of 1.68 on VQA-RAD. These results highlight Med-GLIP's effectiveness in improving Med-VQA performance.

CONCLUSION

We present Med-GLIP, a unified and modality-aware framework for medical image grounding, together with Med-GLIP-5M—a large-scale and diverse grounding dataset. Our approach effectively bridges the semantic gap across imaging modalities and significantly improves downstream tasks such as medical VQA and report generation. Extensive experiments validate its superior grounding accuracy and generalization ability. Med-GLIP demonstrates the potential of scalable, spatially grounded pretraining for building generalizable medical vision-language models, paving the way for broader clinical applications and future integration with large language models.

REFERENCES

- [1] B. Liu, L.-M. Zhan, L. Xu, L. Ma, Y. Yang, and X.-M. Wu, "Slake: A semantically-labeled knowledge-enhanced dataset for medical visual question answering," in 2021 IEEE 18th international symposium on biomedical imaging (ISBI). IEEE, 2021, pp. 1650–1654.
- [2] K. Zou, Y. Bai, Z. Chen, Y. Zhou, Y. Chen, K. Ren, M. Wang, X. Yuan, X. Shen, and H. Fu, "Medrg: Medical report grounding with multi-modal large language model," arXiv preprint arXiv:2404.06798, 2024.
- [3] Z. Chen, Y. Zhou, A. Tran, J. Zhao, L. Wan, G. S. K. Ooi, L. T.-E. Cheng, C. H. Thng, X. Xu, Y. Liu et al., "Medical phrase grounding with region-phrase context contrastive alignment," in *International Conference on Medical Image Computing and Computer-Assisted Intervention*. Springer, 2023, pp. 371–381.
- [4] S. Jiang, T. Zheng, Y. Zhang, Y. Jin, and Z. Liu, "Moe-tinymed: Mixture of experts for tiny medical large vision-language models," arXiv e-prints, pp. arXiv-2404, 2024.
- [5] S. Jiang, T. Zheng, Y. Zhang, Y. Jin, L. Yuan, and Z. Liu, "Med-moe: Mixture of domain-specific experts for lightweight medical vision-language models," arXiv preprint arXiv:2404.10237, 2024.
- [6] S. Jiang, Y. Wang, S. Song, Y. Zhang, Z. Meng, B. Lei, J. Wu, J. Sun, and Z. Liu, "Omniv-med: Scaling medical vision-language model for universal visual understanding," arXiv preprint arXiv:2504.14692, 2025.
- [7] M. Jiang, Q. Huang, L. Zhang, X. Wang, P. Zhang, Z. Gan, J. Diesner, and J. Gao, "Tiger: Text-to-image grounding for image caption evaluation," in *Proceedings of the 2019 Conference on Empirical Methods in Natural Language Processing and the 9th International Joint Conference on Natural Language Processing (EMNLP-IJCNLP)*. Association for Computational Linguistics, 2019.
- [8] R. A. Yeh, M. N. Do, and A. G. Schwing, "Unsupervised textual grounding: Linking words to image concepts," in *Proceedings of the IEEE Conference on Computer Vision and Pattern Recognition*, 2018, pp. 6125–6134.
- [9] X. Chen, Z. Lai, K. Ruan, S. Chen, J. Liu, and Z. Liu, "R-llava: Improving med-vqa understanding through visual region of interest," arXiv preprint arXiv:2410.20327, 2024.
- [10] P. Wang, L. Tong, J. Liu, and Z. Liu, "Fair-moe: Fairness-oriented mixture of experts in vision-language models," arXiv preprint arXiv:2502.06094, 2025.
- [11] S. Jiang, Y. Zhang, C. Zhou, Y. Jin, Y. Feng, J. Wu, and Z. Liu, "Joint visual and text prompting for improved object-centric perception with multimodal large language models," arXiv preprint arXiv:2404.04514, 2024.
- [12] X. Gai, C. Zhou, J. Liu, Y. Feng, J. Wu, and Z. Liu, "Medthink: A rationale-guided framework for explaining medical visual question answering," in *Findings of the Association for Computational Linguistics:* NAACL 2025, 2025, pp. 7438–7450.
- [13] J. Liu, Y. Wang, J. Du, J. Zhou, and Z. Liu, "Medcot: Medical chain of thought via hierarchical expert," in *Proceedings of the 2024 Conference* on *Empirical Methods in Natural Language Processing*, 2024, pp. 17371–17389.
- [14] J. Liu, T. Hu, H. Xiong, J. Du, Y. Feng, J. Wu, J. Zhou, and Z. Liu, "Vpl: Visual proxy learning framework for zero-shot medical image diagnosis," in *Findings of the Association for Computational Linguistics:* EMNLP 2024, 2024, pp. 9978–9992.
- [15] J. Liu, T. Hu, Y. Zhang, Y. Feng, J. Hao, J. Lv, and Z. Liu, "Parameter-efficient transfer learning for medical visual question answering," *IEEE Transactions on Emerging Topics in Computational Intelligence*, vol. 8, no. 4, pp. 2816–2826, 2023.
- [16] J. Liu, T. Hu, J. Du, R. Zhang, J. T. Zhou, and Z. Liu, "Kpl: Training-free medical knowledge mining of vision-language models," arXiv preprint arXiv:2501.11231, 2025.
- [17] K. Sun, S. Xue, F. Sun, H. Sun, Y. Luo, L. Wang, S. Wang, N. Guo, L. Liu, T. Zhao et al., "Medical multimodal foundation models in clinical diagnosis and treatment: Applications, challenges, and future directions," arXiv preprint arXiv:2412.02621, 2024.
- [18] W. Khan, S. Leem, K. B. See, J. K. Wong, S. Zhang, and R. Fang, "A comprehensive survey of foundation models in medicine," *IEEE Reviews* in *Biomedical Engineering*, 2025.
- [19] T. Zheng, J. Liu, Y. Feng, J. Lv, and Z. Liu, "Refined individual tooth segmentation from cone beam ct images," in 2024 IEEE International Symposium on Biomedical Imaging (ISBI). IEEE, 2024, pp. 1–5.

- [20] L. Tong, J. Liu, Y. Feng, T. Hu, and Z. Liu, "Tsnet: Integrating dental position prior and symptoms for tooth segmentation from cbct images," in *Medical Imaging with Deep Learning, short paper track*, 2023.
- [21] J. Liu, J. Hao, H. Lin, W. Pan, J. Yang, Y. Feng, G. Wang, J. Li, Z. Jin, Z. Zhao et al., "Deep learning-enabled 3d multimodal fusion of conebeam ct and intraoral mesh scans for clinically applicable tooth-bone reconstruction," *Patterns*, vol. 4, no. 9, 2023.
- [22] Y. Xie, C. Zhou, L. Gao, J. Wu, X. Li, H.-Y. Zhou, S. Liu, L. Xing, J. Zou, C. Xie et al., "Medtrinity-25m: A large-scale multimodal dataset with multigranular annotations for medicine," arXiv preprint arXiv:2408.02900, 2024.
- [23] C. Li, C. Wong, S. Zhang, N. Usuyama, H. Liu, J. Yang, T. Naumann, H. Poon, and J. Gao, "Llava-med: Training a large language-and-vision assistant for biomedicine in one day," *Advances in Neural Information Processing Systems*, vol. 36, pp. 28541–28564, 2023.
- [24] C. Wu, X. Zhang, Y. Zhang, Y. Wang, and W. Xie, "Medklip: Medical knowledge enhanced language-image pre-training for x-ray diagnosis," in *Proceedings of the IEEE/CVF International Conference on Computer Vision*, 2023, pp. 21372–21383.
- [25] J. Ma, Y. He, F. Li, L. Han, C. You, and B. Wang, "Segment anything in medical images," *Nature Communications*, vol. 15, no. 1, p. 654, 2024.
- [26] A. Kirillov, E. Mintun, N. Ravi, H. Mao, C. Rolland, L. Gustafson, T. Xiao, S. Whitehead, A. C. Berg, W.-Y. Lo et al., "Segment anything," in *Proceedings of the IEEE/CVF international conference on computer vision*, 2023, pp. 4015–4026.
- [27] L. L. Chepelev, D. Kwan, C. E. Kahn, R. W. Filice, and K. C. Wang, "Ontologies in the new computational age of radiology: Radlex for semantics and interoperability in imaging workflows," *RadioGraphics*, vol. 43, no. 3, p. e220098, 2023.
- [28] M. Everingham, S. M. A. Eslami, L. Van Gool, C. K. I. Williams, J. Winn, and A. Zisserman, "The pascal visual object classes challenge: A retrospective," *International Journal of Computer Vision*, vol. 111, no. 1, pp. 98–136, Jan. 2015.
- [29] L. H. Li, P. Zhang, H. Zhang, J. Yang, C. Li, Y. Zhong, L. Wang, L. Yuan, L. Zhang, J.-N. Hwang et al., "Grounded language-image pre-training," in *Proceedings of the IEEE/CVF conference on computer* vision and pattern recognition, 2022, pp. 10965–10975.
- [30] J. Devlin, M.-W. Chang, K. Lee, and K. Toutanova, "Bert: Pre-training of deep bidirectional transformers for language understanding," arXiv preprint arXiv:1810.04805, 2018.
- [31] J. Cheng, B. Fu, J. Ye, G. Wang, T. Li, H. Wang, R. Li, H. Yao, J. Chen, J. Li et al., "Interactive medical image segmentation: A benchmark dataset and baseline," arXiv preprint arXiv:2411.12814, 2024.
- [32] A. E. Johnson, T. J. Pollard, S. J. Berkowitz, N. R. Greenbaum, M. P. Lungren, C.-y. Deng, R. G. Mark, and S. Horng, "Mimic-cxr, a deidentified publicly available database of chest radiographs with free-text reports," *Scientific data*, vol. 6, no. 1, p. 317, 2019.
- [33] Z. Huang, X. Zhang, and S. Zhang, "Kiut: Knowledge-injected utransformer for radiology report generation," in *Proceedings of the IEEE/CVF conference on computer vision and pattern recognition*, 2023, pp. 19809–19818.
- [34] J. J. Lau, S. Gayen, A. Ben Abacha, and D. Demner-Fushman, "A dataset of clinically generated visual questions and answers about radiology images," *Scientific data*, vol. 5, no. 1, pp. 1–10, 2018.
- [35] X. He, Y. Zhang, L. Mou, E. Xing, and P. Xie, "Pathvqa: 30000+ questions for medical visual question answering," arXiv preprint arXiv:2003.10286, 2020.
- [36] Z. Chen, Y. Song, T. Chang, and X. Wan, "Generating radiology reports via memory-driven transformer," CoRR, 2020.
- [37] K. Liu, Z. Ma, X. Kang, Y. Li, K. Xie, Z. Jiao, and Q. Miao, "Enhanced contrastive learning with multi-view longitudinal data for chest x-ray report generation," 2025. [Online]. Available: https://arxiv.org/abs/2502.20056
- [38] C. Li, C. Wong, S. Zhang, N. Usuyama, H. Liu, J. Yang, T. Naumann, H. Poon, and J. Gao, "Llava-med: Training a large language-and-vision assistant for biomedicine in one day," 2023. [Online]. Available: https://arxiv.org/abs/2306.00890
- [39] Z. Zong, G. Song, and Y. Liu, "Detrs with collaborative hybrid assignments training," in *Proceedings of the IEEE/CVF international* conference on computer vision, 2023, pp. 6748–6758.